Pectin methylesterase activity is required for RALF1 peptide signalling output

Ann-Kathrin Rößling[1,2], Kai Dünser[1,3], Chenlu Liu[1,2], Susan Lauw[4,5], Marta Rodriguez-Franco[6], Lothar Kalmbach[1], Elke Barbez[1,2,#], Jürgen Kleine-Vehn[1,2,3,#]

[1]Institute of Biology II, Molecular Plant Physiology (MoPP), University of Freiburg, 79104 Freiburg, Germany

[2]Center for Integrative Biological Signalling Studies (CIBSS), University of Freiburg, 79104 Freiburg, Germany

[3]Institute of Molecular Plant Biology (IMPB), Department of Applied Genetics and Cell Biology, University of Natural Resources and Life Sciences (BOKU), Vienna, 1190 Vienna, Austria

[4]Core Facility Signalling Factory & Robotics, University of Freiburg, Germany

[5]Centre for Biological Signalling Studies (BIOSS), University of Freiburg, 79104 Freiburg, Germany

[6]Institute of Biology II, Cell Biology, University of Freiburg, 79104 Freiburg, Germany

[#]Correspondence should be addressed to juergen.kleine-vehn@biologie.uni-freiburg.de or elke.barbez@cibss.uni-freiburg.de

Abstract:

The extracellular matrix plays an integrative role in cellular responses in plants, but its contribution to the signalling of extracellular ligands largely remains to be explored. RAPID ALKALINIZATION FACTORs (RALFs) are extracellular peptide hormones that play pivotal roles in various physiological processes. Here, we address a crucial connection between the de-methylesterification machinery of the cell wall component pectin and RALF1 activity. Pectin is a polysaccharide, contributing to the structural integrity of the cell wall. Our data illustrate that the pharmacological and genetic interference with PECTIN METHYL ESTERASEs (PMEs) abolishes RALF1-induced root growth repression. Our data suggest that positively charged RALF1 peptides bind negatively charged, de-methylesterified pectin with high avidity. We illustrate that the RALF1 association with de-methylesterified pectin is required for its FERONIA-dependent perception, contributing to the control of the extracellular matrix and the regulation of plasma membrane dynamics. Notably, this mode of action is independent of the FER-dependent extracellular matrix sensing mechanism provided by FER interaction with the Leucine-Rich Repeat Extensin (LRX) proteins. We propose that the methylation status of pectin acts as a contextualizing signalling scaffold for RALF peptides, linking extracellular matrix dynamics to peptide hormone-mediated responses.

Introduction:

Plants perceive various external signals, but how signals interact with the extracellular matrix is poorly understood. Pectin is a heteropolysaccharide, primarily composed of galacturonic acid units, contributing to the mechanical strength and integrity of the cell wall. Pectin (homogalacturonan) plays a vital role in growth control with an emerging role in signalling (Wolf, 2022). In the cell wall, PECTIN METHYL ESTERASEs (PMEs) catalyse the removal of methyl groups from the initially esterified pectin, giving rise to negatively charged carboxylic acid groups and altering the interaction of pectin with various extracellular components (Peaucelle et al., 2008). Here we address how the methylation status of pectin in the extracellular matrix contributes to the integration of RAPID ALKALINIZATION FACTORs (RALFs), which are extracellular cysteine-rich plant peptide hormones. RALF peptides are involved in multiple physiological and developmental processes, ranging from organ and pollen tube growth to the modulation of immune responses (Stegmann et al., 2017; Abarca et al., 2021, Mecchia et al., 2017, Ge et al., 2017). Catharanthus roseus receptor-like kinase 1-like (CrRLK1L) are transmembrane proteins with an extracellular domain, consisting of two adjacent malectin-like domains, for RALF signal perception and a cytoplasmic kinase domain for intracellular signal transduction (Escobar-Restrepo et al, 2007). FERONIA (FER) is currently the best characterized CrRLK1L, contributing to the above-mentioned developmental programs as well as the integration of environmental cues (Feng et al., 2018; Gigli-Bisceglia et al., 2022). On a cellular level, RALF binding to FER leads to rapid apoplastic (extracellular) alkalinisation (Haruta et al., 2014), which modulates cell wall properties, ion fluxes, and enzymatic activities, thereby influencing cellular expansion rates (Haruta et al., 2014; Barbez et al., 2017; Dünser et al., 2019). Besides its role in apoplastic pH, CrRLK1Ls play a role in cell wall sensing (Hematy et al., 2007; Höfte, 2015; Shih et al., 2014) and can bind to extracellular pectin (Feng et al., 2018; Lin et al., 2022, Liu et al., 2024). The FER-dependent cell wall sensing mechanism involves the direct interaction with the extracellular LEUCINE-RICH REPEAT EXTENSINs (LRXs) in roots (Dünser et al., 2019), suggesting that LRXs provide a physical link between FER and the cell wall (Herger et al., 2019). On the other hand, root, as well as pollen-expressed LRX proteins, also bind to RALF peptides (Mecchia et al., 2017; Dünser et al., 2019; Moussu et al., 2020), but its contribution to mechanochemical sensing and/or growth control is largely unknown in roots. Here we show that the PME-dependent de-methylesterification status of pectin defines the FER-dependent perception of RALF1, contributing to extracellular regulation of pH, cell wall and plasma membrane remodelling, control of receptor endocytosis as well as organ growth in roots. Our data suggests

that negatively charged, de-methylesterified pectin binds to positively charged RALF1 peptides with low affinity but high avidity. Interference with the de-methylesterification of pectin, out-titrating RALF1 with small charged, de-methylesterified pectin fragments, as well as the disruption of the positive charges in RALF1, abolishes the RALF1 activity in roots. We accordingly propose that the RALF interaction with de-methylesterified pectin at the root surface is crucial for its FER-dependent perception in roots. Even though root-expressed LRX proteins are strictly required for the FER-dependent mechano-sensing in roots, the LRX proteins are not essential for RALF perception in roots (Dünser et al., 2019). We moreover show here that LRX proteins do not contribute to the integration of RALF-pectin signalling in roots. In conclusion, we report on the crucial contribution of pectin de-methylesterification, for FER-dependent RALF peptide hormone signalling in root growth control. Our work proposes that pectin acts as a context-dependent extracellular signalling scaffold, contributing to signalling dynamics at the plasma membrane.

Results and discussion:

The application of RALF1 peptides induces strong repression of main root growth in *Arabidopsis thaliana* (Haruta et al., 2014; Figure 1A, B), which we initially used here as a bioassay to visualise RALF1 activity. To assess if the de-methylesterification status of pectin may impact peptide signalling, we pharmacologically interfered with the de-methylesterification of pectin, using epigallocatechin gallate (EGCG). EGCG is a natural inhibitor of PME activity (Lewis et al., 2008) and its application lowered main root growth but its co-treatment markedly interfered with the RALF1-induced reduction in root growth (Figure 1A, B). In contrast, the structurally similar epicatechin (EC) is not an inhibitor of PMEs (Lewis et al., 2008) and did not block RALF1-induced root growth repression (Figure 1C, D). In agreement, EGCG but not EC application reduced the labelling of de-methyl esterified pectin in roots (Figure 1E, F) as visualised by the fluorescent probe COS^{488} (Mravec et al., 2014). This set of data suggests that the EGCG-induced interference with PME activity correlates with reduced RALF1 responses in roots. To consolidate this assumption, we employed the overexpression of *PECTIN METHYLESTERASE INHIBITOR* (*PMEI3*), which is well characterised to interfere with PME activity (Peaucelle et al., 2008) and accordingly also reduced the extracellular de-methylesterification of pectin in epidermal root cells (Figure 1G, H). In agreement with the EGCG application, *PMEI3,* as well as *PMEI5,* gain-of-function reduced the RALF1-induced root growth repression (Figure 1I, J).

We accordingly conclude that pharmacological and genetic interference with PME activity leads to the repression of RALF1 effects on root growth. To test the specificity of this effect, we subsequently used the peptide flagellin22 (flg22). The flg22 peptide is derived from the N-terminus of bacterial flagellin and is known to elicit root growth repression via the innate immune receptor FLAGELLIN SENSITIVE2 (FLS2) (Chinchilla et al., 2006). EGCG treatments were not able to suppress, but additively enhanced the FLG22-induced root growth repression (Figure 1K, L), suggesting a rather specific effect of PME inhibition on balancing RALF1 activity.

Next, we addressed how PME activity affects RALF1-dependent root growth control. FER-dependent perception of RALF peptides may affect cell wall integrity and it is hence conceivable that the pharmacological and genetic interference with extracellular PME activity could counterbalance some extracellular effects of RALF1 signalling. Using electron microscopy, we indeed observed a RALF1-induced effect on cell wall integrity, showing swollen cell walls, but also revealed plasma membrane invaginations (Figure 2A, B). These pronounced RALF effects were to our knowledge never reported and hence we confirmed these effects independently, using live cell confocal imaging. RALF1-induced invaginations of plasma membrane markers, such as Low-Temperature inducible protein 6b (LTi6b) (Figure 2C) and Novel Plant SNARE 12 (NPSN12) (SFigure 1A), were readily detectable. Similarly, confocal imaging of propidium iodide (PI)-stained cell walls of wild-type seedlings also depicted the RALF1-induced swelling of the apoplastic signal and revealed additional ectopic accumulations (Figure 2D, F). These RALF1-induced alterations were absent in PI-stained *fer-4* loss-of-function mutants (Figure 2E, F), suggesting that FER activation is required for these cellular effects of RALF1. The pharmacological (Figure 2G, H) as well as genetic (Figure 2I-K) interference with PME activity abolished the RALF1-induced alterations in cell wall labelling, phenocopying *fer-4* mutants.

PME activity could hence either indirectly counterbalance RALF1 effects on the cell wall and/or it could directly define RALF1 signalling output in root cells. Accordingly, we next tested the RALF1 impact on apoplastic pH regulation, which is a primary readout of RALF1 perception by FER (Haruta et al., 2014). We used 8-hydroxypyrene-1,3,6-trisulfonic acid trisodium salt (HPTS) as a fluorescent pH indicator for assessing apoplastic pH in epidermal root cells (Barbez et al., 2017). As expected, the application of RALF1 peptides induced an extracellular pH alkalization in wild-type epidermal root cells (Barbez et al., 2017; Figure 3A, B). In contrast, EGCG application (Figure 3A, B) as well as the overexpression of PMEI3 (Figure 3C, D), abolished the RALF-induced alkalization of the apoplastic pH. We accordingly

conclude that interference with PME activity disrupts the primary output signalling of RALF1 in root cells.

Our data suggests that PME inhibition interferes with RALF1 signalling output, ultimately affecting cell wall properties and root growth. To assess if PME activity affects the extracellular perception of RALF1, we next investigated the ligand-induced cellular dynamics of its receptor FER. An early event of receptor-mediated signalling often involves the ligand-induced endocytosis of the receptor as has been previously demonstrated for the RALF1-receptor FER (Yu et al., 2020). Therefore, we next tested whether the RALF1 ligand-induced endocytosis of FER is altered upon changes in the methylation status of pectin. In agreement with previous reports, we observed the RALF1-induced internalization of functional *FER::FER-GFP* in epidermal root cells (Figure 3F, G). On the other hand, the ligand-induced internalization of FER-GFP was abolished when we pharmacologically or genetically suppressed PME activity (Figure 3F-J). These findings propose that the PME activity is required for the earliest events of RALF1 perception by FER in roots.

To test the specificity of this observation, we used another RALF peptide called RALF34, which is a ligand of CrRLK1L THESEUS1 (THE1) (Gonneau et al., 2018). Similar to RALF1, the application of RALF34 induced the internalisation of FER-GFP, which was fully suppressed when PME activity was inhibited (SFigure 2A, B). Therefore, we assume that several RALF peptides display the same or similar signalling modalities.

RALF peptides are positively charged (Abarca et al., 2021). It is hence conceivable that the association of positively charged RALF1 peptides with de-methylesterified, negatively charged pectin is required for its FER-dependent perception. To indirectly assess if RALF1 peptides bind de-methylesterified pectin, we tested if RALF1 peptides bind fragments of de-methylesterified oligogalacturonides (OGs).

We initially assessed potential OG binding to RALF1, using the RALF1 impact on root cells as a bio-assay. The addition of high levels of free, de-methylesterified OGs into the media did not visibly affect the cell wall or FER endocytosis on its own (SFigure 3A-D). On the other hand, free OGs in the medium strongly interfered with RALF1-induced cell wall swelling and FER receptor endocytosis in roots (SFigure 3A-D). This effect was concentration-dependent (Figure 4A, B), suggesting that excess of de-methylesterified OGs in the medium can bind and out-titrate RALF1 peptides and thereby limit the RALF1 activity at the root surface.

To characterise this binding *in vitro*, we next used biotinylated RALF1 in biolayer interferometry (BLI), which is an optical technique for measuring macromolecular interactions by analyzing interference patterns of white light reflected from the surface of a biosensor tip.

The equilibrium dissociation constant (Kd) in the range of 105 nanomolar (nM) (Figure 4C) suggests a physiologically relevant binding affinity. Notably, we however observed an initial OG association to RALF1 with a constant (K_{on}) in the micromolar (µM) range, but the dissociation kinetics revealed a remarkably slow rate (Figure 4C, D). This is indicative of relatively low affinity at the individual RALF1-OG binding event level but multiple intermolecular binding events may eventually lead to a high accumulative binding strength. We hence propose that RALF1 peptides and de-methylesterified OGs undergo low affinity but high avidity binding assemblies. This finding complements recent data, indicating that the binding of RALF peptides and de-methylesterified OGs leads to phase separation *in vitro* (Liu et al., 2024).

RALF1 contains in total 8 positively charged amino acids (3 lysine (K) and 5 arginine (R)) (SFigure 4A, B). This is reminiscent of the well-characterised de-methylesterified pectin-binding protein POLYGALACTURONASE-INHIBITING PROTEIN (PGIP), which binds to de-methylesterified pectin through a positively charged binding site formed by clustered residues of lysine (K) and arginine (R) (Spadoni et al., 2006). Notably, the LRX8-RALF4 complex binds de-methylesterified OGs in a charge-dependent manner in pollen (Moussu et al., 2023). To address the positive charges in RALF1, we synthesized a RALF1-like peptide by substituting the K and R residues (*RALF1*$^{-KR}$). Thereby, we created a slightly negatively charged peptide in the pH range of the cell wall (SFigure 4A, C). *RALF1*$^{-KR}$ peptides are not bioactive, because they did neither affect root growth, nor cell wall integrity, nor did they induce the ligand-induced endocytosis of FER in epidermal root cells (SFigure 4D-I). These findings suggest that the positively charged residues in RALF1 are essential for its activity in roots. Even though we cannot rule out that *RALF1*$^{-KR}$ affects several characteristics of RALF1 signalling, we used this non-charged peptide to test if these residues affect the RALF1 binding to de-methylesterified pectin. Using our *in vitro* system, we did not observe *RALF1*$^{-KR}$ binding to de-methylesterified OGs (SFigure 4J), proposing that RALF1 and OGs indeed interact in a charge-dependent manner.

The LRX-RALF complex and its interaction with pectin exerts a condensing effect on the cell wall in pollen and root hairs (Moussu et al., 2023; Schoenaers et al., 2024). Moreover, LRX proteins also bind and link FER with a cell wall-sensing mechanism in roots (Dünser et al., 2019). Nevertheless, LRX function in root growth appears to be independent of FER-dependent RALF signalling (Dünser et al., 2019). Hence, we next tested if LRX proteins are required for the joint RALF1/pectin-dependent signalling in roots. We observed that RALF1 applications still induced cell wall alterations in *lrx1 lrx2 lrx3 lrx4 lrx5* quintuple mutant roots

(Figure 5A-D). Similar to wild-type roots (Figure 5E, F), pharmacological interference with PME activity still repressed RALF1 activity in the *lrx1 lrx2 lrx3 lrx4 lrx5* quintuple mutant roots (Figure 5G, H). These findings confirm our previous assumptions that LRX proteins are not essential for the RALF activity in roots (Dünser et al., 2019) and, moreover, reveal that LRX proteins are also not required for the PME-dependent control of RALF1 signalling in roots.

In conclusion, our data proposes that RALF1 peptides are associated with high avidity to de-methyl esterified pectin, which is required for the RALF perception by FER. We hence conclude that the methylation status of pectin provides a conceptualising input to RALF peptide hormone signalling (Figure 5I, J).

Concluding remarks:

Intriguingly, the exogenous application of RALF1 does not only affect cell wall characteristics but also induces prominent plasma membrane protrusions into root epidermal cells. Plasma membrane invagination is a highly controlled process and often relates to plant endosymbiotic events (Su et al., 2023). The developmental importance of this RALF1 effect remains to be addressed but could pinpoint pectin signalling playing a central role in the structural coordination of cell wall and plasma membrane dynamics. Most importantly, we reveal an essential function of the cell wall component pectin for RALF1 peptide signalling (Figure 5I, J). We illustrate that the pharmacological and genetic interference with PME activity specifically abolishes RALF1, but not flg22 peptide, activity in roots. We conclude that PME activity is required for all hallmarks of RALF1 signalling, including the rapid alkalinisation of the cell wall and the ligand-induced endocytosis of FER. We hence propose that the generation of de-methylesterified, negatively charged pectin in the cell wall is required for the FER-dependent perception of positively charged RALF1 at the root cell surface. We show that RALF1 binds in a charge-dependent manner to de-methylesterified OGs *in vitro* and that the application of free OGs can out-titrate RALF1 peptides in the medium. Our *in vitro* data proposes low affinity but a high avidity binding of OGs and RALF1. This interaction mechanism could be key in the spatial enrichment of RALF peptides at the root surface because receptor interactions at the plasma membrane could contribute to the accumulated strength of multiple binding interactions. In agreement, after we pre-printed a previous version of this manuscript (Rößling et al., bioRxiv 2023), Moussu and colleagues proposed that the LRX8-RALF4 complex and its charge-dependent binding of de-methylesterified OGs controls extracellular condensations in pollen tubes (Moussu et al., 2023). The contribution of FER

signalling remains unknown in this process, but a similar structural mechanism defines root hair growth in a FER-dependent manner (Schoenaers et al., 2024). Within the main root, the RALF peptide binding to de-methylesterified pectin was suggested to be sufficient to lead to its extracellular phase separation, subsequently inducing the clustering of FER receptors in the plasma membrane (Liu et al., 2024). It remained however unknown if LRX proteins are implied in this root organ growth response. LRX proteins directly interact with FER and thereby contribute to cell wall sensing in roots (Dünser et al., 2019). Notably, LRX proteins are not required to sense RALF1 in roots (Dünser et al., 2019) and also the inhibition of PMEs still represses RALF1 activity in *lrx1 lrx2 lrx3 lrx4 lrx5* quintuple mutant roots. These findings suggest an LRX-independent mode of action in the FER-RALF1-pectin signalling mechanism. Our findings (this study and Dünser et al., 2019) pinpoint distinct FER- and RALF-dependent roles of LRX proteins. Considering that LRX8-RALF4-pectin interaction contributes to wall integrity and pollen tube expansion (Moussu et al., 2023), distinct modes of cell wall integrity control may be also in place in root cells and tip-growing pollen tubes.

Based on our findings, we envision that negatively charged, de-methylesterified pectin could function as a signalling scaffold for positively charged RALF peptides, which seems crucial for its signalling via the FER receptor. It needs to be seen how precisely the RALF binding to homogalacturonan affects its interaction with FER receptors. Here it is noteworthy that the pectin sensing function of FER is physically separated from the RALF binding domain (Gronnier et al., 2022).

The impact of de-methylesterified pectin on RALF signalling could also lead to self-emerging feedback properties because high extracellular PME activity is expected to strongly acidify the apoplast (Wolf et al., 2009), which in turn would be counteracted by the de-methylesterified pectin-induced activation of RALF peptides and its consequences on apoplast alkalinisation (Haruta et al., 2014; Barbez et al., 2017; this study). The here uncovered mechanism links the pectin-related cell wall status with RALF peptide hormone signalling. A scaffold protein can tether signalling components, enhancing the efficiency and specificity of cellular signalling pathways by acting as a structural framework. In analogy, we propose that pectin functions in a PME-dependent manner as a tunable extracellular signalling scaffold.

Figure legends

Figure 1. PME activity is required for RALF1-induced root growth repression

(A-B) Three-day-old wild-type seedlings were subjected for three days to 1 µM RALF1 and/or 2.5 µM EGCG (A). (B) Boxplots depict the root length of wild-type seedlings under different treatments shown in (A).

(C-D) Three-day-old wild-type seedlings were transferred for three days to solvent control, 1 µM RALF1 and/or 15 µM EC (C). (D) Boxplots depict root length of wild-type seedlings under different treatments shown in (C).

(E-F) Confocal microscopy images of the root epidermal cells of 6-day-old wild-type seedlings after 3 h treatment in liquid medium with 50 µM EC/EGCG or solvent control. Seedlings were stained with COS^{488} to visualize de-methylesterified pectin. (F) Boxplots displaying the probe staining signal intensity shown in (E). Scale bar = 25 µm, n = 8-10 roots per treatment with a total number of 79 - 96 quantified cells.

(G-H) Confocal microscopy images of the root epidermal cells of 6-day-old wild-type and *PMEI3-OE* seedlings, stained with COS^{488} to visualize de-methylesterified pectin. (H) Boxplots displaying the probe staining signal intensity shown in (G). Scale bar = 25 µm, n = 9 - 11 roots per treatment with 71 - 77 quantified cells.

(I-J) Three-day-old wild-type, *PMEI3-OE* and *PMEI5-OE* seedlings were exposed for three days to 1 µM RALF1 or solvent control (I). (J) Boxplots depict the root length of wild-type compared to *PMEI3-OE* seedlings of the treatments shown in (I).

(K-L) Three-day-old wild-type seedlings were exposed for three days with 0.5 µM flg22 and 15 µM EGCG or solvent control (K). (L) Boxplots depict the root length of wild-type seedlings under different treatments shown in (K).

Statistical significance was determined by a one-way ANOVA with a Tukey Post Hoc multiple comparisons test ($P < 0.05$, letters indicate significance categories) (B, D, F, J and L) and a student´s t-test (***p = 0.0001) (H). Boxplots: Box limits are representing the 25th and 75th percentile, the horizontal line represents the median. Whiskers display min. to max. values. Representative experiments are shown. (A, C, I, K) Scale bar = 1 cm, n = 11- 13 roots per treatment/line.

Figure 2. RALF1 requires PME activity to affect cell wall integrity

(A-B) Representative transmission electron microscopy (TEM) images of epidermal root cells treated for 3 h with solvent control and 1 µM RALF1, respectively. Arrowheads indicate RALF1-induced plasma membrane invaginations. Scale bar = 10 µm. (B) shows details, Scale bar = 2 µm.

(C) Confocal microscopy images of the root epidermal cells of 6-day-old LTI6b-YFP expressing seedlings, treated for 3 h with solvent control or 1 µM RALF1. Scale bar = 25 µm.
(D-F) Confocal microscopy images of the root epidermal cells of 6-day-old wild-type (D) and *fer-4* mutant (E) seedlings, treated for 3 h with 1 µM RALF1 or solvent control. Seedlings were mounted in propidium iodide to visualize the cell walls. Arrowheads indicate RALF1-induced alterations of the cell wall stain. (F) Graphs represent the width of PI signal per root under different treatments shown in (D, E). Scale bar = 25 µm, n = 9 – 11 roots per treatment with a total number of 49 – 51 quantified cells.
(G-H) Confocal microscopy images (G) and quantification (H) of 6-day-old roots of wild-type seedlings, treated in liquid medium with 1 µM RALF1 and/or 50 µM EGCG as well as solvent control for 3 h. Seedlings were mounted in propidium iodide to visualize the cell walls. Arrowheads indicate cell wall invaginations. Scale bar = 25 µm, n = 8 – 10 roots per treatment with a total number of 44 – 49 quantified cells.
(I-K) Confocal microscopy images (I, J) and quantification (K) of 6-day-old wild-type (I) and *PMEI3-OE* (J) roots, treated in liquid medium with 1 µM RALF1 or solvent control for 3 h. Seedlings were mounted in propidium iodide to visualize the cell walls. Arrowheads indicate cell wall invaginations. Scale bar = 25 µm, n = 8 – 12 roots per treatment with a total number of 46 – 53 quantified cells.
Statistical significance was determined by a one-way ANOVA with a Tukey Post Hoc multiple comparisons test ($P < 0.05$, letters indicate significance categories) (H) or a two-way ANOVA with Bonferroni Post Hoc test (**** = $P < 0.0001$) (F and K). Boxplots: Box limits are representing the 25th and 75th percentile, the horizontal line represents the median. Whiskers display min. to max. values.

Figure 3. PME activity is required for RALF1 signalling output

(A-B) HPTS-based (458/405 ratio) pH assessment of late meristematic root cells of wild-type seedlings treated for 3h with 1 µM RALF1, 50 µM ECGC or both compared to solvent control. Representative confocal images (A) are shown. Scale bar = 10 µm. (B) Boxplots depict mean HPTS 458/405 intensities shown in (A), n = 9 – 11.
(C-D) HPTS-based (458/405 ratio) pH assessment of late meristematic cells in wild-type and *PMEI3-OE* seedlings treated for 3h with 1 µM RALF1 compared to solvent control. Scale bar = 10 µm. (D) Boxplots depict mean HPTS 458/405 intensities shown in (C), n = 10 – 12.

(F-G) RALF1-induced internalization of *FER::FER-GFP* in late meristematic epidermal root cells of seedlings treated for 3h with 1 µM RALF1, 50 µM ECGC or both compared to solvent control. Scale bar = 25 µm. (G) Boxplots displaying the mean intracellular GFP signal intensity shown in (F), n = 9 – 12.

(H-J) RALF1-induced internalization of FER in late meristematic epidermal root cells in *FER::FER-GFP* (H) and in *FER::FER-GFP* crossed with *PMEI3-OE* (I) seedlings treated for 3h with 1 µM RALF1 compared to solvent control. Scale bar = 25 µm. (J) Boxplots displaying the intracellular GFP signal intensity shown in (H and I).

Statistical significance was determined by a one-way ANOVA with a Tukey Post Hoc multiple comparisons test ($P < 0.05$, letters indicate significance categories) (B and G) or a two-way ANOVA with Bonferroni Post Hoc test (**** = $P < 0.0001$) (D and J). Boxplots: Box limits are representing 25th and 75th percentile, the horizontal line represents the median. Whiskers display min. to max. values.

Figure 4. RALF peptides associate with de-methylesterified oligogalacturonides

(A-B) RALF1-induced internalization of *FER::FER-GFP* in late meristematic epidermal root cells of six-day-old seedlings treated for 3h with a concentration series of 0.5, 1 and 1.5 µM RALF1 compared to solvent control and co-treated with OGs with a chain length of 25-50 (OG^{25-50}; 50 mg/mL). (B) Boxplots displaying the mean intracellular GFP signal intensity are shown in (A). Scale bar = 25 µm, n = 9 – 12.

(C-D) Biolayer interferometry assays showed the binding between RALF1 and OG^{25-50} with an Equilibrium dissociation constant (Kd) of 105 nM (C). The association and dissociation constants (k_{ON} = 1.02 x 103 M-1 s-1, k_{OFF} _=1.07 x 10-4 s-1) imply high avidity binding (D).

Statistical significance was determined by a one-way ANOVA with a Tukey Post Hoc multiple comparisons test ($P < 0.05$, letters indicate significance categories) (B). Boxplots: Box limits are representing 25th and 75th percentile, the horizontal line represents the median. Whiskers display min. to max. values.

Figure 5. LRX proteins are not essential for the PME-dependent activity of RALF1

(A-B) Confocal microscopy images (A) and quantification (B) representing the average cell wall width per root under different treatments shown in (A), of 6-day-old roots of wild-type seedlings, treated in liquid medium with 1 µM RALF1 and/or 50 µM EGCG as well as solvent control for 3 h. Seedlings were mounted in propidium iodide to visualize the cell walls.

Arrowheads indicate cell wall invaginations. Scale bar = 25 µm, n = 10 – 12 roots per treatment with a total number of 44 – 52 quantified cells.

(C-D) Confocal microscopy images (C) and quantification (D) representing the average cell wall width per root under different treatments shown in (C), of 6-day-old roots of *lrx1/lrx2/lrx3/lrx4/lrx5* quintuple mutant seedlings, treated in liquid medium with 1 µM RALF1 and/or 50 µM EGCG as well as solvent control for 3 h. Seedlings were mounted in propidium iodide to visualize the cell walls. Arrowheads indicate cell wall invaginations. Scale bar = 25 µm, n = 11 – 12 roots per treatment with a total number of 46 – 53 quantified cells.

(E-H) Three-day-old wild-type (E) or *lrx1/lrx2/lrx3/lrx4/lrx5* quintuple mutant (G) seedlings transferred for three days in liquid growth medium supplemented with solvent control, 1 µM RALF1 and/or 15 µM EGCG. Seedlings were transferred to solid growth medium just before imaging. (F, H) Boxplots display root length of seedlings under different treatments shown in (E, G). Scale bar = 1 cm, n = 14 – 16 roots per treatment/line.

(I-J) De-methylesterified and hence negatively charged pectin is crucial for the signalling output of positively charged RALF peptides (I). Interference with PME activity, application of free de-methylesterified OGs, or removal of positive charges in RALF leads to abolished RALF1 output signalling (J).

Statistical significance was determined by a one-way ANOVA with a Tukey Post Hoc multiple comparisons test ($P < 0.05$, letters indicate significance categories) (B, D, F and H). Boxplots: Box limits are representing 25th and 75th percentile, the horizontal line represents the median. Whiskers display min. to max. values. Representative experiments are shown.

Figure S1. Cell wall invaginations after RALF1 treatment in a plasma membrane marker

(A) Confocal images of epidermal cells in 6-day-old roots of the plasma membrane marker *UBQ10::NPSN12-YFP* after 3 h treatment in liquid medium with solvent control or 1 µM RALF1. Scale bar = 25 µm, n = 10 – 13.

Figure S2. RALF34 function is similar to RALF1 in initiating ligand-induced endocytosis in FER

(A-B) Internalization of *FER::FER-GFP* in late meristematic epidermal root cells of six-day-old seedlings treated for 3h with 1 µM RALF1, 1 µM RALF34 and/or 50 µM EGCG compared to solvent control. (B) Boxplots displaying the mean intracellular GFP signal intensity are

shown in (A). Scale bar = 25 µm, n = 10 – 12 roots per treatment with a total number of 41 – 46 quantified cells.
Statistical significance was determined by a one-way ANOVA with a Tukey Post Hoc multiple comparisons test ($P < 0.05$, letters indicate significance categories) (B, D, F and H). Boxplots: Box limits are representing 25th and 75th percentile, the horizontal line represents the median. Whiskers display min. to max. values. Representative experiments are shown.

Figure S3. Application of free de-methylesterified oligogalacturonides disrupts RALF1 activity at the cell surface

(A-B) Confocal images of 6-day-old wild-type roots after 3 h treatment in liquid medium with solvent control, 50 mg/mL OG^{10-15}, 50 mg/mL OG^{25-50} and 1 µM RALF1, respectively (A). Seedlings were mounted in propidium iodide to visualize the cell walls. Arrowheads indicate cell wall invaginations. (B) Graphs represent the average cell wall width per root under different treatments shown in (A). Scale bar = 25 µm, n = 8 – 11 roots per treatment with a total number of 46 – 52 quantified cells.
(C-D) RALF1-induced internalization of *FER::FER-GFP* in late meristematic epidermal root cells of 6-day-old seedlings treated for 3h with solvent control, 50 mg/mL OG^{10-15}, 50 mg/mL OG^{25-50} and 1 µM RALF1, respectively. (D) Boxplots display the intracellular FER-GFP signal intensities. Scale bar = 25 µm, n = 10 – 11.
Statistical significance was determined by a one-way ANOVA with a Tukey Post Hoc multiple comparisons test ($P < 0.05$, letters indicate significance categories) (B and D). Boxplots: Box limits represent 25th and 75th percentile, and the horizontal line represents the median. Whiskers display min. to max. values. Representative experiments are shown.

Figure S4. Positive charges in RALF1 are required for its bioactivity

(A-C) Amino acid composition of RALF1 and non-charged $RALF1^{-KR}$ peptides and its respective pH-dependent net charge (B, C).
(D-E) Three-day-old wild-type seedlings were exposed for three days to 1 µM RALF1 or $RALF1^{-KR}$ or solvent control (D). (E) Boxplots display root length of seedlings under different treatments shown in (D). Scale bar = 1 cm, n = 14 – 15.
(F-G) Representative confocal images of 6-day-old wild-type roots after 3 h treatment in liquid medium with 1 µM RALF1 or $RALF1^{-KR}$ or solvent control. Seedlings were mounted in propidium iodide to visualize the cell walls. Arrowheads indicate cell wall invaginations (F).

(G) Graphs represent the average cell wall width per root under different treatments shown in (F). Scale bar = 25 µm, n = 9 – 12.

(H-I) RALF1-induced internalization of *FER::FER-GFP* in late meristematic epidermal root cells of 6-day-old seedlings treated for 3h with solvent control, 1 µM RALF1 or RALF1^{-KR}. Representative confocal images (H) are shown.. (I) Boxplots display the intracellular GFP signal intensity. Scale bar = 25 µm, n = 11 – 12 roots per treatment with a total number of 50 – 56 quantified cells.

(J) Biolayer interferometry assays showed the absence of binding between RALF1^{-KR} and OG$^{25-50}$. RALF1 was used as a positive control, exhibiting the binding as appeared in the previous measurements (see Fig. 4D).

Statistical significance was determined by a one-way ANOVA with a Tukey Post Hoc multiple comparisons test ($P < 0.05$, letters indicate significance categories) (E, G and I). Boxplots: Box limits are representing 25th and 75th percentile, the horizontal line represents the median. Whiskers display min. to max. values. Representative experiments are shown.

Material and methods

Plant material and growth conditions

All experiments were carried out in *Arabidopsis thaliana*, ecotype *Col-0*. The following plant lines were described in previous publications: *PMEI3-OE* (Peaucelle et al., 2008), *PMEI5-OE* (Wolf et al., 2014), *lrx1/lrx2/lrx3/lrx4/lrx5* (Dünser et al., 2019), *LTI6b-YFP* (Cutler et al., 2000), *UBQ10::NPSN12-YFP* (Wave131Y, Geldner et al., 2009), *FER::FER-GFP* (in *fer-4*, Shih et al., 2014), *fer-4* (Shih et al., 2014), *FER::FER-GFP* x *PMEI3-OE* (in *fer-4*, obtained by crossing). After surface sterilization in 70% and 100% ethanol, seeds were vernalized at 4°C for 2 days in darkness, afterwards grown vertically on ½ strength Murashige and Skoog (MS) medium plates containing 1% sucrose in a long-day regime (16 h light and 8 h darkness) at 21 °C.

Chemicals and peptides

All chemicals were dissolved in dimethyl sulfoxide (DMSO) and served as solvent control, unless indicated otherwise. We used Propidium iodide (PI) in a working concentration of 0.02 mg/mL for cell wall counterstaining (obtained from Sigma (MO, USA)). Epigallocatechin gallate (EGCG) was used to interfere with PME activity in liquid treatments (obtained from

Cayman Chemical (MI, USA)), epicatechin (EC) was used as negative control (from Cayman Chemical (MI, USA)) and flg22 peptides as a peptide control (obtained from Sigma (MO, USA)). The RALF1 peptide (mature RALF1, with the amino acid sequence: ATTKYISYQSLKRNSVPCSRRGASYYNCQNGAQANPYSRGCSKIARCRS) and the non-charged RALF1^{-KR} peptide version (amino acid sequence: ATTSYISYQSLTSNSVPCSDTGASYYNCQNGAQANPYSDGCSYIASCRS) were both synthesized by PSL GmbH (Heidelberg, Germany) and dissolved in water. The galacturonan oligosaccharides OG$^{10-15}$ and OG$^{25-50}$ were obtained from Elicityl (Crolles, France) and Biosynth (Staad, Switzerland), respectively.

Confocal microscopy

For image acquisition, an upright Leica TCS SP8 FALCON FLIM confocal laser scanning microscope, equipped with a Leica HC PL APO Corr 63 x 1.20 water immersion CS2 objective, was used. GFP was excited at 488 nm (fluorescence emission: 500 - 550 nm), PI at 561 nm (fluorescence emission: 640 - 750 nm). Experiments assessing apoplastic pH were carried out as previously described (Barbez et al., 2017) using 8-hydroyypyrene-1,3,6-trisulfonuc acid trisodium salt (HPTS; Sigma-Aldrich). In brief, roots of 6-day-old seedlings were treated for 3 h in liquid ½ MS medium containing 1 µM RALF1 and/or 50 µM EGCG or the appropriate amount of solvent control (water or DMSO, respectively) for 3 h. For the RALF1-OG titration experiment, 0.5, 1 and 1.5 µM RALF1 were mixed with OG$^{25-50}$ in a concentration of 50 mg/mL and the seedlings were incubated for 3 h. If not mentioned otherwise, pharmacological treatments have been performed in liquid medium in multiwell plates. Prior to imaging, the roots were mounted on a solid block of ½ MS medium containing 1 mM HPTS. The block was transferred to a microscopy slide and imaged with a coverslip on top. Image processing was performed as previously described (Barbez et al., 2017) using a macro for Fiji. Four transversal cell walls were quantified per root. The protonated form of HPTS was excited at 405 nm and 0.5% Diode UV laser intensity, and the deprotonated form at 455 nm with 30% Argon laser intensity. Images here were obtained in sequential scan mode. Z-stacks were recorded with a step size of 420 nm, with a stack containing 20 slices on average. The Gain of the HyD detectors (or PMT for HPTS experiments) stayed constant during imaging. The pinhole was set to 111.4 µm (for HPTS experiments to 196 µm). To counterstain the cell walls, roots were mounted in PI solution (0.02 mg/mL) prior to imaging. The signal intensity of intracellular space or plasma membrane was assessed using Fiji, with four cells analyzed per root. The ROI stayed constant over the experiments and biological replicates. For

quantification of the PI staining width (and therefore the thickness of the cell wall) the thickness of transversal and longitudinal sections stained by PI were measured using Fiji, with four to six stained plasma membranes quantified per root. For the RALF1-treated roots, only the invaginated regions were chosen for analysis.

Synthesis of COS probes

The COS probe was generated as described in Mravec et al., 2014, using chitosan oligosaccharides conjugated with AlexaFluor 488 hydroxylamine (ThermoFisher, Waltham, Massachusetts, USA). In brief, 1 mg/ml oligosaccharide solution was mixed into 0.1 M sodium acetate buffer, pH 4.9. The AlexaFluor 488 (10 mg/ml in DMSO) was added to the oligosaccharide (½ of the moles of the oligosaccharide). After incubation at 37°C for 48 h with shaking at 1,400 rpm the probe was ready. 6- day-old seedlings were transferred into liquid ½ MS medium and supplemented with DMSO, 50 µM EGCG and EC for 3 hours respectively. After the treatment, seedlings were staining in liquid ½ MS medium supplemented with COS^{488} at a 1:500 dilution, for 30 min, and washed twice with medium. Imaging of root tips was performed directly afterwards.

Root length analysis and root growth assay

For root growth assays, seedlings were grown for 3 days on solid ½ MS plates. Afterwards, they were transferred into 3 mL of liquid ½ MS medium containing RALF1 and/or EGCG or the appropriate amount of solvent control (water or DMSO, respectively). After 3 days of growth in liquid media with gentle agitation on a platform shaker, the seedlings were placed on solid ½ MS plates and scanned using a flatbed scanner. Root length was measured using Fiji. For statistical analyses, the GraphPad Prism Software (version 9.5.1) was used.

Sample preparation for electron microscopy

6-day-old wild-type seedlings were treated for 3 h in liquid ½ MS media containing solvent control or 1 µM RALF1. After the treatment, roots were cut apart with a razor blade, immediately submerged in MTSB buffer containing 4% p-formaldehyde (PFA) and vacuum infiltrated for 15 minutes in a microwave oven (Pelco BioWave Pro+) at room temperature. The submerged roots were left in the fixative solution for 4 h at room temperature and overnight at 4°C. All further steps were performed according to Dünser et al. (2022).

In silico analysis

For assessment of the charge of the RALF1 and RALF1^{-KR} peptide, the Peptide Calculator Online tool from https://www.biosynth.com/peptide-calculator was used.

Biolayer interferometry assays

Octet@RED 96 was used to perform the binding assay between the biotinylated RALF1 or biotinylated RALF1^{-KR} and OG$^{25-50}$. Both, biotinylated-RALF1 and biotinylated RALF1^{-KR} (purchased from Peptide Specialty Laboratory GmbH) were solubilized in DMSO as a stock solution in a concentration of 11 mg/ml. The buffer used for the interaction was PBS pH 7.4 containing 25 µg/ml BSA. RALF1 was used as a positive control to compare the binding of RALF1^{-KR} to OG$^{25-50}$. The Blank contained the biotinylated ligand without OG$^{25-50}$.

Test experiments were carried out to rule out the unspecific binding of OG$^{25-50}$ to the streptavidin biosensor and biotin. The Streptavidin biosensor was first dipped in the interaction buffer for 600 s continued by loading with 5 µg/ml Biotinylated-RALF1 as a ligand for 600 s. The sensors were washed in the interaction buffer for 600 s followed by OG$^{25-50}$ in the concentration of 0, 0.5, 1, 2, 3, 4 and 5 µM for association (600 s). Finally, dissociation was monitored for 600 s in the interaction buffer. Three biological replicates were measured and analyzed using Octet Red Data Analysis software version 8.0.2.3. The fitting curve was selected to be a 1:1 binding model. The curves were plotted using GraphPad Prism6 software.

Illustrations

The summary figures (Fig. 5 I, J) were created using the Concepts App for iOS (Version 6.9.2, TopHatch, Inc. (Turku, Finnland)) and edited using AffinityDesigner (version 1.10, Serif (West Bridgford, UK)) by Ann-Kathrin Rößling.

Acknowledgements

We are grateful to Niko Geldner, Gabriele Monshausen, Grégory Mouille, and Jozef Mravec for sharing published material; our team members for helpful discussions; and the LIC Imaging Center Freiburg for expertise and support. We would like to thank Rosula Hinnenberg of the EM facility at the Faculty of Biology, University of Freiburg, for her assistance with the generation of EM data. The TEM (Hitachi HT7800) was funded by the DFG grant (project number 426849454). This work was supported by the Austrian Science Fund (FWF) (P33044

to J.K-V.,), and the German Science Fund (DFG; 470007283 to J.K.-V. and CIBSS – EXC-2189 Project ID 390939984 to J.K.-V. and to E.B.).

References

Abarca, A., Franck, C. M., & Zipfel, C. (2021). Family-wide evaluation of rapid alkalinization factor peptides. *Plant Physiology*, *187*(2), 996–1010. https://doi.org/10.1093/plphys/kiab308

Barbez, E., Dünser, K., Gaidora, A., Lendl, T., & Busch, W. (2017). Auxin steers root cell expansion via apoplastic pH regulation in Arabidopsis thaliana. *PNAS*, E4884–E4893. https://doi.org/10.5061/dryad.sq7s3

Chinchilla, D., Zipfel, C., Robatzek, S., Kemmerling, B., Nürnberger, T., Jones, J. D. G., Felix, G., & Boller, T. (2007). A flagellin-induced complex of the receptor FLS2 and BAK1 initiates plant defence. *LETTERS* , *447*, 497–501. https://doi.org/10.1038/nature05999

Cutler, S. R., Ehrhardt, D. W., Griffitts, J. S., & Somerville, C. R. (2000). Random GFP::cDNA fusions enable visualization of subcellular structures in cells of Arabidopsis at a high frequency. *PNAS*, *97*(7), 3718–3723. www.pnas.org.

Dünser, K., Gupta, S., Herger, A., Feraru, M. I., Ringli, C., & Kleine-Vehn, J. (2019). Extracellular matrix sensing by FERONIA and Leucine-Rich Repeat Extensins controls vacuolar expansion during cellular elongation in Arabidopsis thaliana. *The EMBO Journal*, *38*(7). https://doi.org/10.15252/embj.2018100353

Dünser, K., & Kleine-Vehn, J. (2015). Differential growth regulation in plants-the acid growth balloon theory. In *Current Opinion in Plant Biology* (Vol. 28, pp. 55–59). Elsevier Ltd. https://doi.org/10.1016/j.pbi.2015.08.009

Ge, Z., Bergonci, T., Zhao, Y., Zou, Y., Du, S., Liu, M.-C., Luo, X., Ruan, H., García-Valencia, L. E., Zhong, S., Hou, S., Huang, Q., Lai, L., Moura, D. S., Gu, H., Dong, J., Wu, H.-M., Dresselhaus, T., Xiao, J., … Qu, -Jia. (2017). Arabidopsis pollen tube integrity and sperm release are regulated by RALF-mediated signaling. *Plant Science*, *358*, 1596–1600. Geldner, N., Dénervaud-Tendon, V., Hyman, D. L., Mayer, U., Stierhof, Y.-D., & Chory, J. (2009). Rapid, combinatorial analysis of membrane compartments in intact plants with a multicolor marker set. In *Plant J* (Vol. 59, Issue 1).

Gigli-Bisceglia, N., van Zelm, E., Huo, W., Lamers, J., & Testerink, C. (2022). Arabidopsis root responses to salinity depend on pectin modification and cell wall sensing. *Development (Cambridge)*, *149*(12). https://doi.org/10.1242/dev.200363

Gonneau, M., Desprez, T., Martin, M., Doblas, V. G., Bacete, L., Miart, F., Sormani, R., Hématy, K., Renou, J., Landrein, B., Murphy, E., Van De Cotte, B., Vernhettes, S., De Smet, I., & Höfte, H. (2018). Receptor Kinase THESEUS1 Is a Rapid Alkalinization Factor 34 Receptor in Arabidopsis. *Current Biology*, *28*(15), 2452-2458.e4. https://doi.org/10.1016/j.cub.2018.05.075

Gronnier, J., Franck, C. M., Stegmann, M., Defalco, T. A., Abarca, A., von Arx, M., Dünser, K., Lin, W., Yang, Z., Kleine-Vehn, J., Ringli, C., & Zipfel, C. (2022). Regulation of immune receptor kinase plasma membrane nanoscale organization by a plant peptide hormone and its receptors. *ELife*, *11*. https://doi.org/10.7554/eLife.74162

Haruta, M., Sabat, G., Stecker, K., Minkoff, B. B., & Sussman, M. R. (2014). A peptide hormone and its receptor protein kinase regulate plant cell expansion. *Science*, *343*(6169), 408–411. https://doi.org/10.1126/science.1244454

Hématy, K., Sado, P. E., Van Tuinen, A., Rochange, S., Desnos, T., Balzergue, S., Pelletier, S., Renou, J. P., & Höfte, H. (2007). A Receptor-like Kinase Mediates the Response of Arabidopsis Cells to the Inhibition of Cellulose Synthesis. *Current Biology*, *17*, 922–931.

Herger, A., Dünser, K., Kleine-Vehn, J., & Ringli, C. (2019). Leucine-Rich Repeat Extensin Proteins and Their Role in Cell Wall Sensing. In *Current Biology* (Vol. 29, Issue 17, pp. R851–R858). Cell Press. https://doi.org/10.1016/j.cub.2019.07.039

Höfte, H. (2015). The Yin and Yang of cell wall integrity control: Brassinosteroid and FERONIA signaling. *Plant and Cell Physiology*, *56*(2), 224–231. https://doi.org/10.1093/pcp/pcu182

Lewis, K. C., Selzer, T., Shahar, C., Udi, Y., Tworowski, D., & Sagi, I. (2008). Inhibition of pectin methyl esterase activity by green tea catechins. *Phytochemistry*, *69*(14), 2586–2592. https://doi.org/10.1016/j.phytochem.2008.08.012

Lin, W., Tang, W., Pan, X., Huang, A., Gao, X., Anderson, C. T., & Yang, Z. (2022). Arabidopsis pavement cell morphogenesis requires FERONIA binding to pectin for activation of ROP GTPase signaling. *Current Biology*, *32*(3), 497-507.e4. https://doi.org/10.1016/j.cub.2021.11.030

Liu, M.-C. J., Yeh, F.-L. J., Yvon, R., Simpson, K., Jordan, S., Chambers, J., Wu, H.-M., & Cheung, A. Y. (2024). Extracellular pectin-RALF phase separation mediates FERONIA global signaling function. *Cell*. https://doi.org/10.1016/j.cell.2023.11.038

Mecchia, M. A., Santos-Fernandez, G., Duss, N. N., Somoza, S. C., Boisson-Dernier, A., Gagliardini, V., Martínez-Bernardini, A., Fabrice, T. N., Ringli, C., Muschietti, J. P., & Grossniklaus, U. (2017). RALF4/19 peptides interact with LRX proteins to control pollen tube growth in Arabidopsis. *Science*, *358*, 1600–1603. https://www.science.org

Moussu, S., Broyart, C., Santos-Fernandez, G., Augustin, S., Wehrle, S., Grossnilaus, U., & Santiago, J. (2020). Structural basis for recognition of RALF peptides by LRX proteins during pollen tube growth. *PNAS*, *117*(13), 7494–7503. https://doi.org/10.1073/pnas.2000100117/-/DCSupplemental

Moussu, S., Kyung Lee, H., Haas, K. T., Broyart, C., Rathgeb, U., De Bellis, D., Levasseur, T., Schoenaers, S., Fernandez, G. S., Grossniklaus, U., Bonnin, E., Hosy, E., Vissenberg, K., Geldner, N., Cathala, B., Höfte, H., & Santiago, J. (2023). Plant cell wall patterning and expansion mediated by protein-peptide-polysaccharide interaction. *Science*, *382*, 719–725. https://www.science.org

Mravec, J., Kračun, S. K., Rydahl, M. G., Westereng, B., Miart, F., Clausen, M. H., Fangel, J. U., Daugaard, M., Cutsem, P. Van, De Fine Licht, H. H., Höfte, H., Malinovsky, F. G., Domozych, D. S., & Willats, W. G. T. (2014). Tracking developmentally regulated post-synthetic processing of homogalacturonan and chitin using reciprocal oligosaccharide probes. *Development (Cambridge)*, *141*(24), 4841–4850. https://doi.org/10.1242/dev.113365

Peaucelle, A., Louvet, R., Johansen, J. N., Höfte, H., Laufs, P., Pelloux, J., & Mouille, G. (2008). Arabidopsis Phyllotaxis Is Controlled by the Methyl-Esterification Status of Cell-Wall Pectins. *Current Biology*, *18*(24), 1943–1948. https://doi.org/10.1016/j.cub.2008.10.065

Schoenaers, S., Lee, H. K., Gonneau, M., Faucher, E., Levasseur, T., Akary, E., Claeijs, N., Moussu, S., Broyart, C., Balcerowicz, D., AbdElgawad, H., Bassi, A., Damineli, D. S. C., Costa, A., Feijó, J. A., Moreau, C., Bonnin, E., Cathala, B., Santiago, J., … Vissenberg, K. (2024). Rapid alkalinization factor 22 has a structural and signalling role in root hair cell wall assembly. *Nature Plants*. https://doi.org/10.1038/s41477-024-01637-8

Shih, H. W., Miller, N. D., Dai, C., Spalding, E. P., & Monshausen, G. B. (2014). The receptor-like kinase FERONIA is required for mechanical signal transduction in Arabidopsis seedlings. *Current Biology*, *24*(16), 1887–1892. https://doi.org/10.1016/j.cub.2014.06.064

Spadoni, S., Zabotina, O., Di Matteo, A., Mikkelsen, J. D., Cervone, F., De Lorenzo, G., Mattei, B., & Bellincampi, D. (2006). Polygalacturonase-inhibiting protein interacts with pectin through a binding site formed by four clustered residues of arginine and lysine. *Plant Physiology*, *141*(2), 557–564. https://doi.org/10.1104/pp.106.076950

Stegmann, M., Monaghan, J., Smakowska-Luzan, E., Rovenich, H., Lehner, A., Holton, N., Belkhadir, Y., & Zipfel, C. (2017). The receptor kinase FER is a RALF-regulated scaffold controlling plant immune signaling. *Science*, *355*(6322), 287–289. https://doi.org/10.1126/science.aal2541

Su, C., Zhang, G., Rodriguez-Franco, M., Hinnenberg, R., Wietschorke, J., Liang, P., Yang, W., Uhler, L., Li, X., & Ott, T. (2023). Transcellular progression of infection threads in Medicago truncatula roots is associated with locally confined cell wall modifications. *Current Biology*, *33*(3), 533-542.e5. https://doi.org/10.1016/j.cub.2022.12.051

Wolf, S. (2022). Annual Review of Plant Biology Cell Wall Signaling in Plant Development and Defense. *Annual Review of Plant Biology*, *73*, 323–353. https://doi.org/10.1146/annurev-arplant-102820

Wolf, S., Rausch, T., & Greiner, S. (2009). The N-terminal pro region mediates retention of unprocessed type-I PME in the Golgi apparatus. *Plant Journal*, *58*(3), 361–375. https://doi.org/10.1111/j.1365-313X.2009.03784.x

Xu, F., Gonneau, M., Faucher, E., Habrylo, O., Lefebvre, V., Domon, J. M., Martin, M., Sénéchal, F., Peaucelle, A., Pelloux, J., & Höfte, H. (2022). Biochemical characterization of Pectin Methylesterase Inhibitor 3 from Arabidopsis thaliana. *The Cell Surface*, *8*. https://doi.org/10.1016/j.tcsw.2022.100080

Yu, M., Li, R., Cui, Y., Chen, W., Li, B., Zhang, X., Bu, Y., Cao, Y., Xing, J., Jewaria, P. K., Li, X., Bhalerao, R. P., Yu, F., & Lin, J. (2020). The RALF1-FERONIA interaction modulates endocytosis to mediate control of root growth in Arabidopsis. *Development (Cambridge)*, *147*(13). https://doi.org/10.1242/dev.189902

Figure 1.

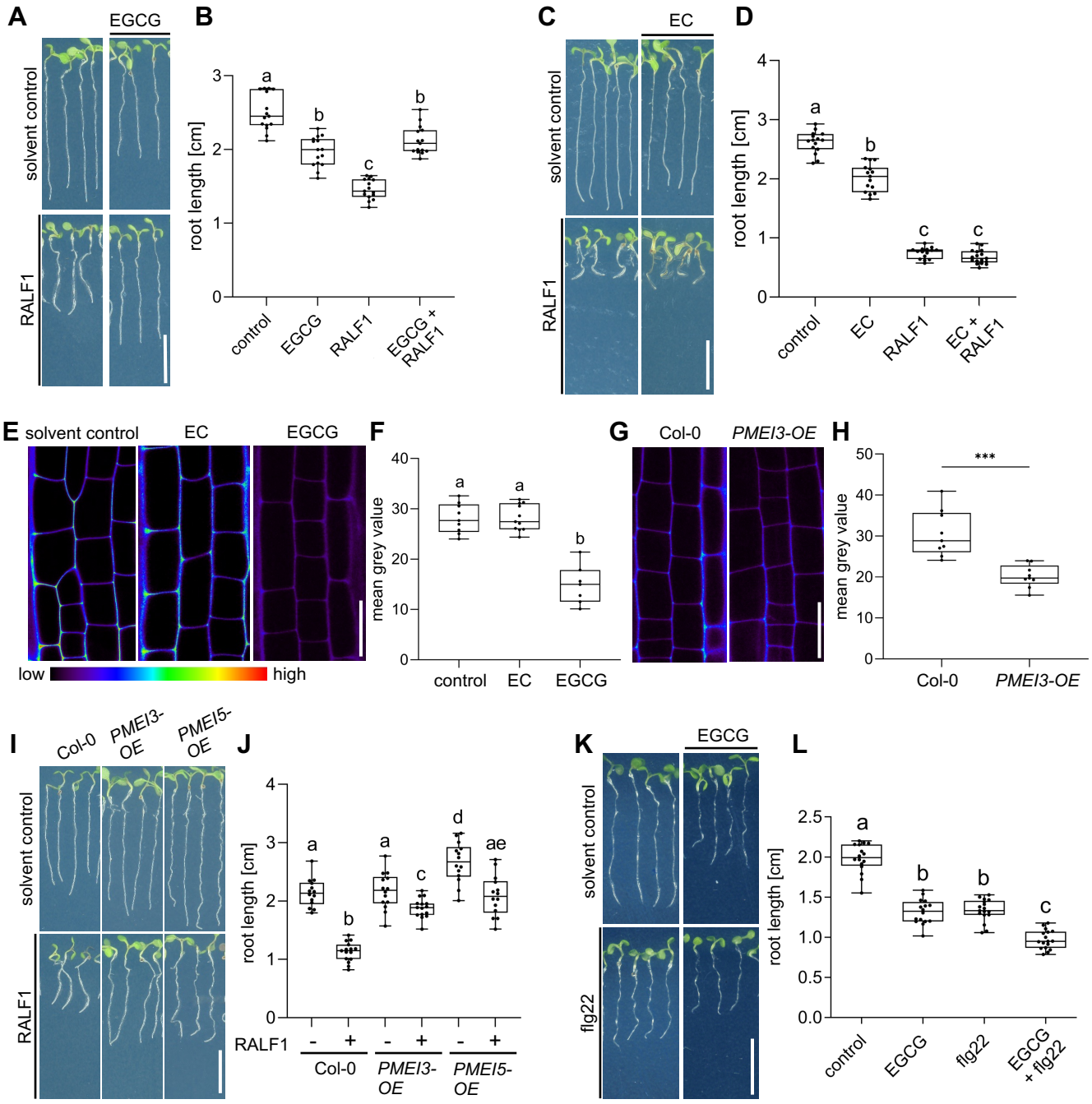
A
EGCG
solvent control
RALF1
B
root length [cm]
control
EGCG
RALF1
EGCG + RALF1
C
EC
D
EC
EC + RALF1
E
solvent control
EC
EGCG
low
high
F
mean grey value
G
Col-0
PMEI3-OE
H
***
I
Col-0
PMEI3-OE
PMEI5-OE
J
RALF1
K
flg22
L
EGCG + flg22

Figure 2.

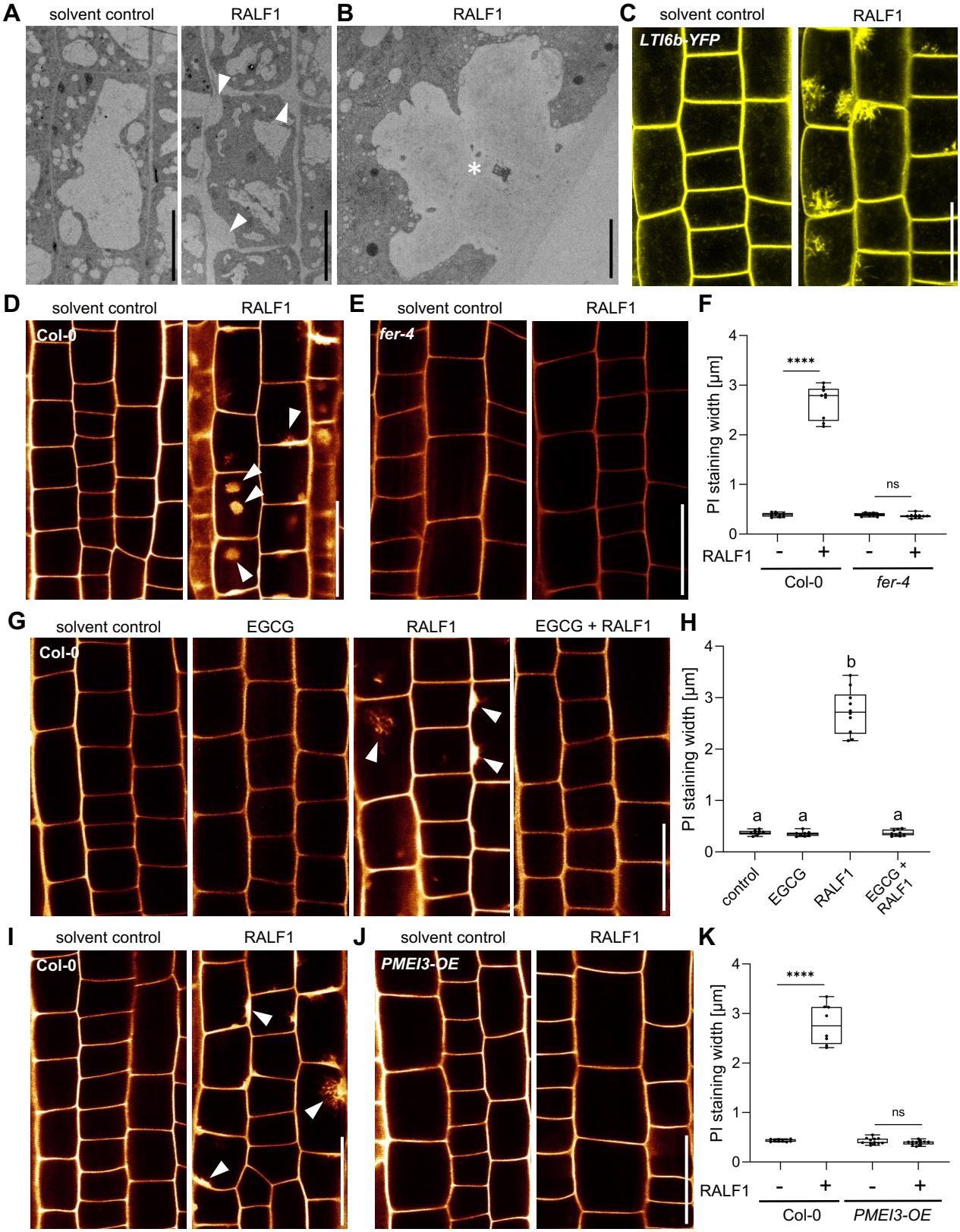
A
solvent control
RALF1
B
RALF1
C
solvent control
RALF1
LTI6b-YFP
D
solvent control
RALF1
Col-0
E
solvent control
RALF1
fer-4
F
PI staining width [µm]
****
ns
RALF1
-
+
-
+
Col-0
fer-4
G
solvent control
EGCG
RALF1
EGCG + RALF1
Col-0
H
PI staining width [µm]
a
a
b
a
control
EGCG
RALF1
EGCG + RALF1
I
solvent control
RALF1
Col-0
J
solvent control
RALF1
PMEI3-OE
K
PI staining width [µm]
****
ns
RALF1
-
+
-
+
Col-0
PMEI3-OE

Figure 3.

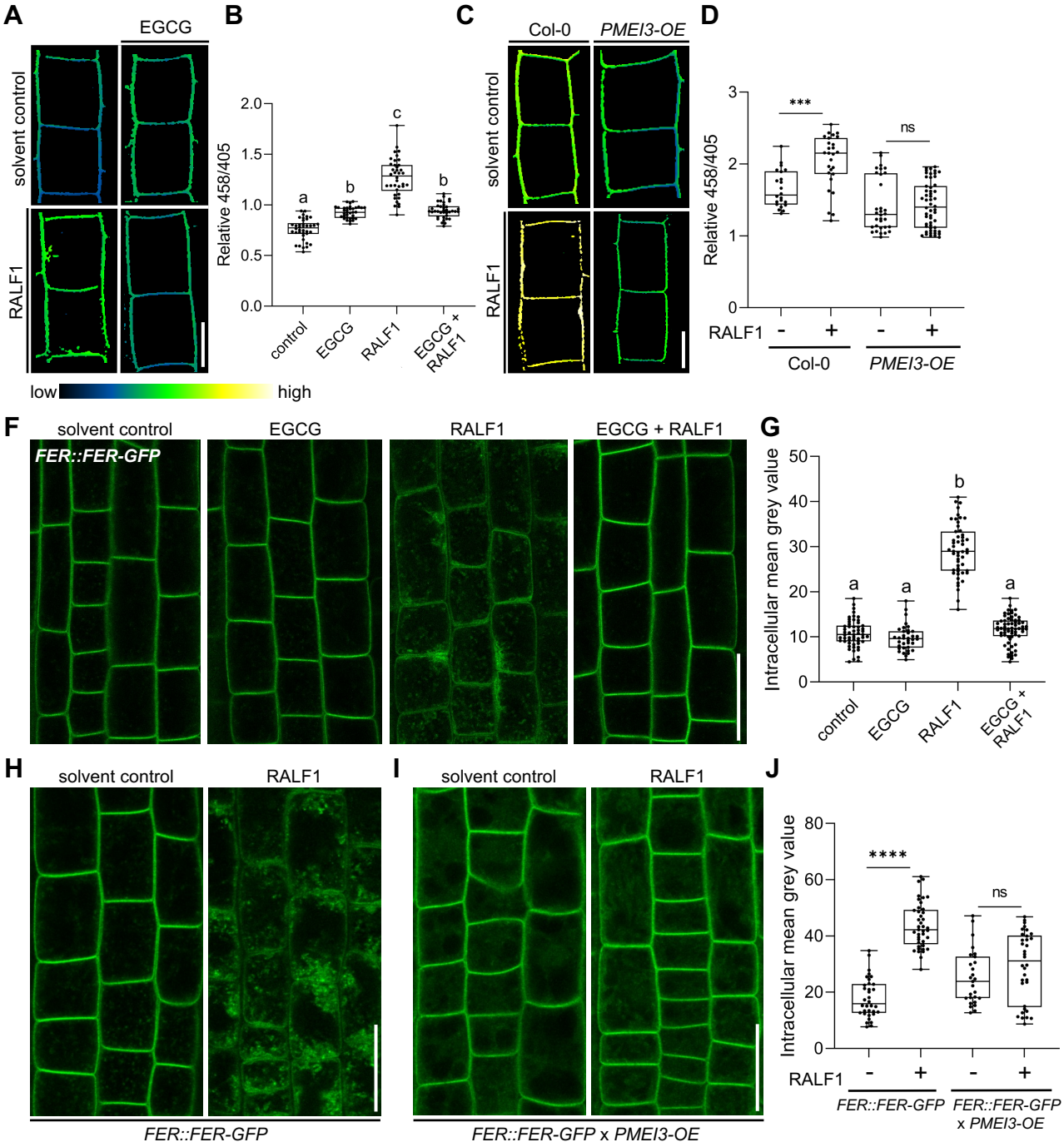
A
EGCG
solvent control
RALF1
low
high
B
Relative 458/405
2.0
1.5
1.0
0.5
0.0
a
b
c
b
control
EGCG
RALF1
EGCG + RALF1
C
Col-0
PMEI3-OE
solvent control
RALF1
D
Relative 458/405
3
2
1
0
***
ns
RALF1
-
+
-
+
Col-0
PMEI3-OE
F
solvent control
EGCG
RALF1
EGCG + RALF1
FER::FER-GFP
G
Intracellular mean grey value
50
40
30
20
10
0
a
a
b
a
control
EGCG
RALF1
EGCG + RALF1
H
solvent control
RALF1
FER::FER-GFP
I
solvent control
RALF1
FER::FER-GFP x PMEI3-OE
J
Intracellular mean grey value
80
60
40
20
0
****
ns
RALF1
-
+
-
+
FER::FER-GFP
FER::FER-GFP x PMEI3-OE

Figure 4.

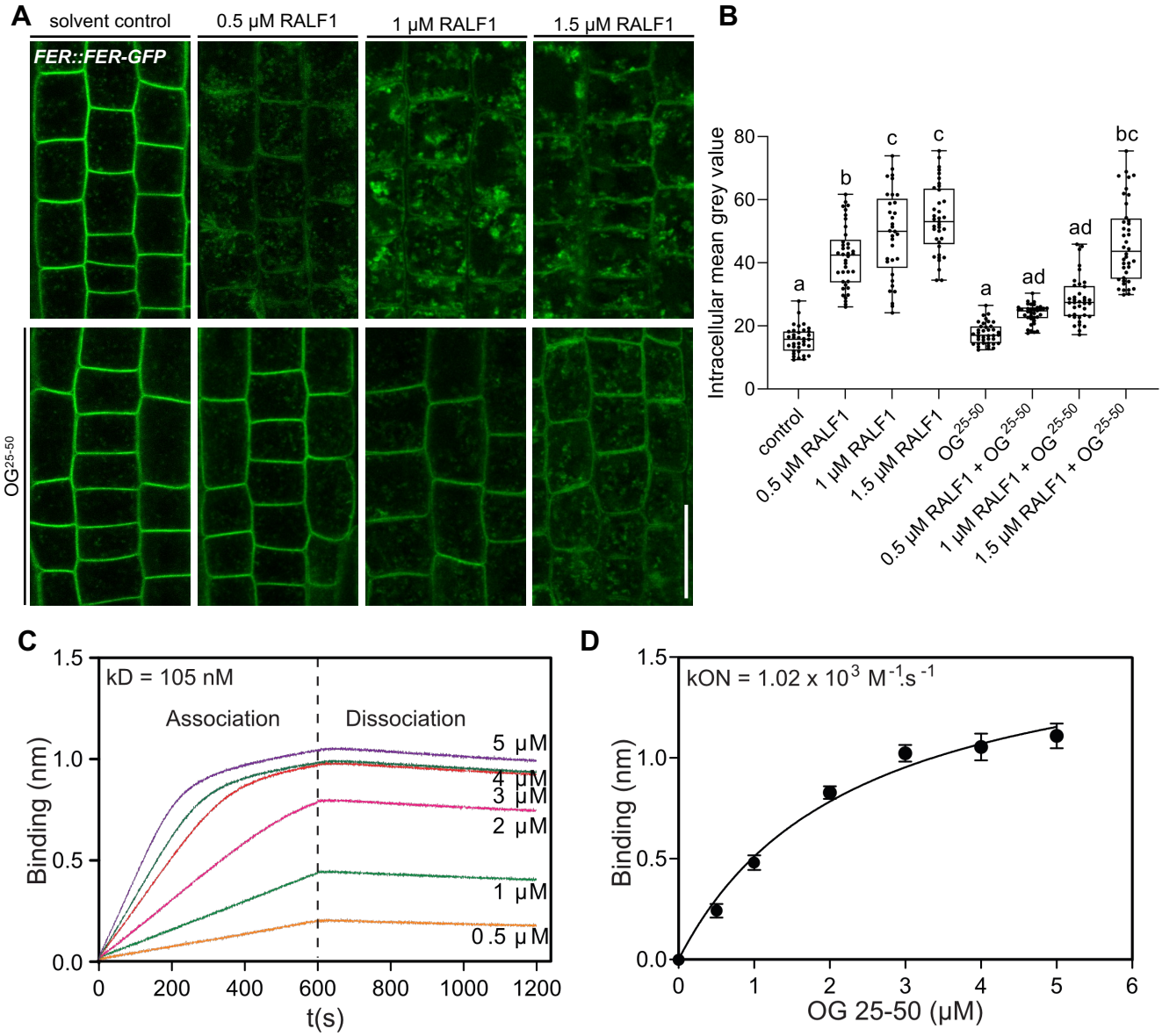
A
solvent control
0.5 µM RALF1
1 µM RALF1
1.5 µM RALF1
FER::FER-GFP
OG25-50
B
Intracellular mean grey value
80
60
40
20
0
a
b
c
c
a
ad
ad
bc
control
0.5 µM RALF1
1 µM RALF1
1.5 µM RALF1
OG 25-50
0.5 µM RALF1 + OG 25-50
1 µM RALF1 + OG 25-50
1.5 µM RALF1 + OG 25-50
C
kD = 105 nM
Association
Dissociation
5 µM
4 µM
3 µM
2 µM
1 µM
0.5 µM
Binding (nm)
1.5
1.0
0.5
0.0
0
200
400
600
800
1000
1200
t(s)
D
kON = 1.02 x 10^3 M^-1.s^-1
Binding (nm)
1.5
1.0
0.5
0.0
0
1
2
3
4
5
6
OG 25-50 (µM)

Figure 5.

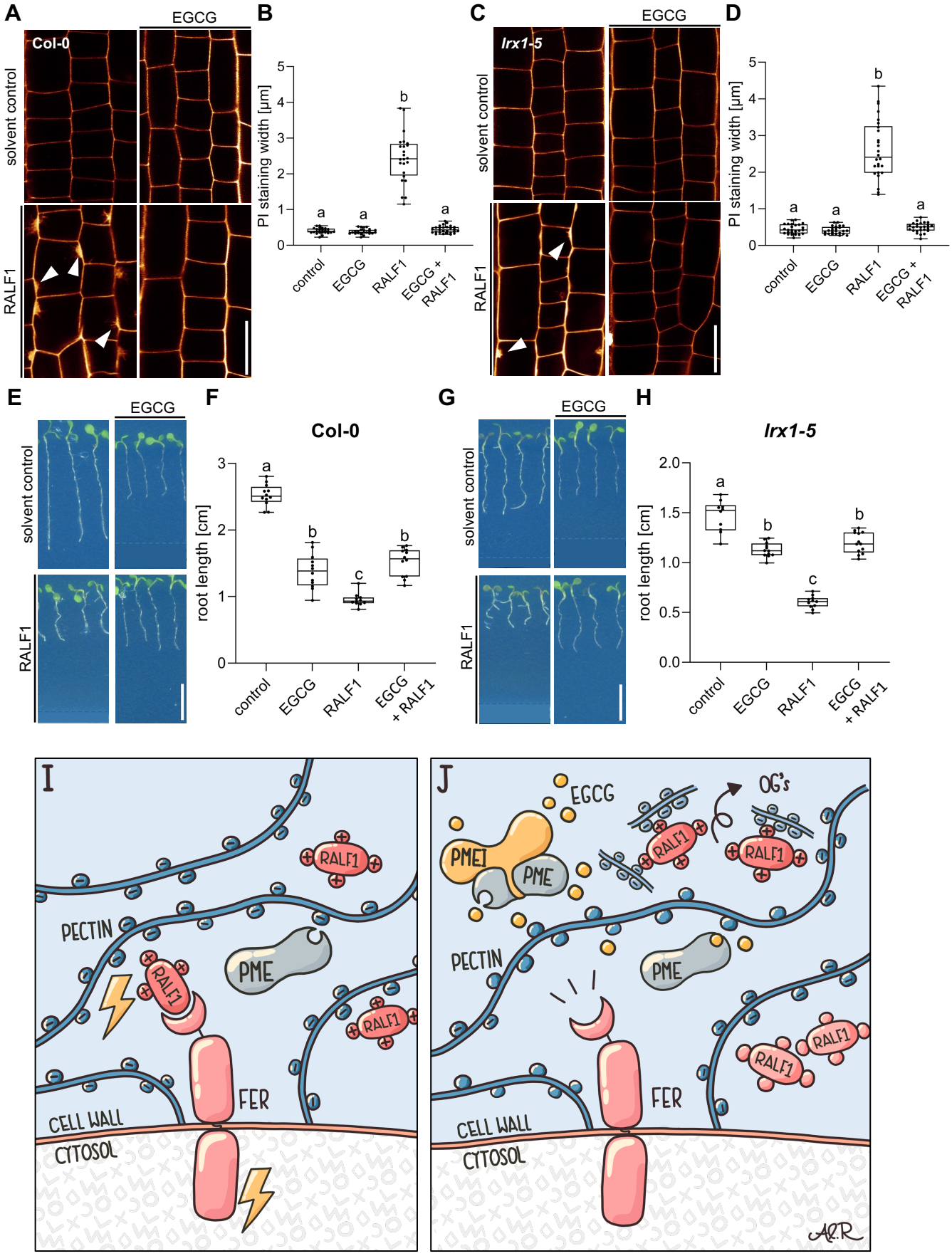
A
EGCG
Col-0
solvent control
RALF1
B
PI staining width [µm]
control
EGCG
RALF1
EGCG + RALF1
C
EGCG
Irx1-5
solvent control
RALF1
D
PI staining width [µm]
control
EGCG
RALF1
EGCG + RALF1
E
EGCG
solvent control
RALF1
F
Col-0
root length [cm]
control
EGCG
RALF1
EGCG + RALF1
G
EGCG
solvent control
RALF1
H
Irx1-5
root length [cm]
control
EGCG
RALF1
EGCG + RALF1
I
RALF1
PECTIN
PME
FER
CELL WALL
CITOSOL
J
EGCG
OG's
PMEI
PME
RALF1
PECTIN
FER
CELL WALL
CITOSOL
A.R.

Figure S1.

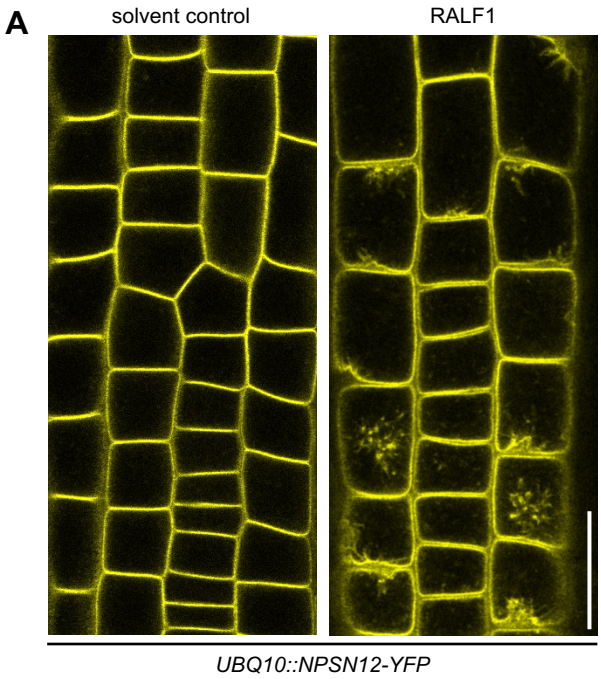

Figure S2.

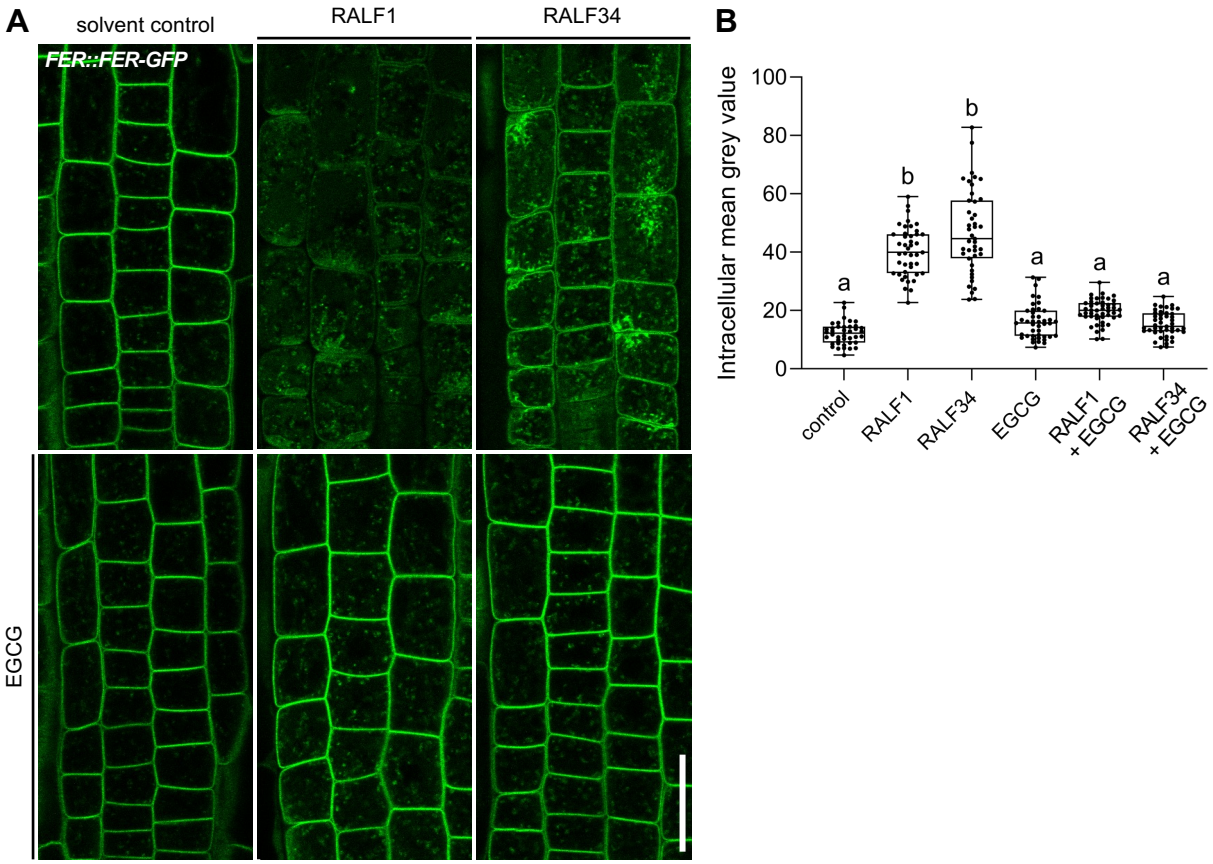
A
solvent control
RALF1
RALF34
FER::FER-GFP
EGCG
B
Intracellular mean grey value
100
80
60
40
20
0
a
b
b
a
a
a
control
RALF1
RALF34
EGCG
RALF1 + EGCG
RALF34 + EGCG

Figure S3.

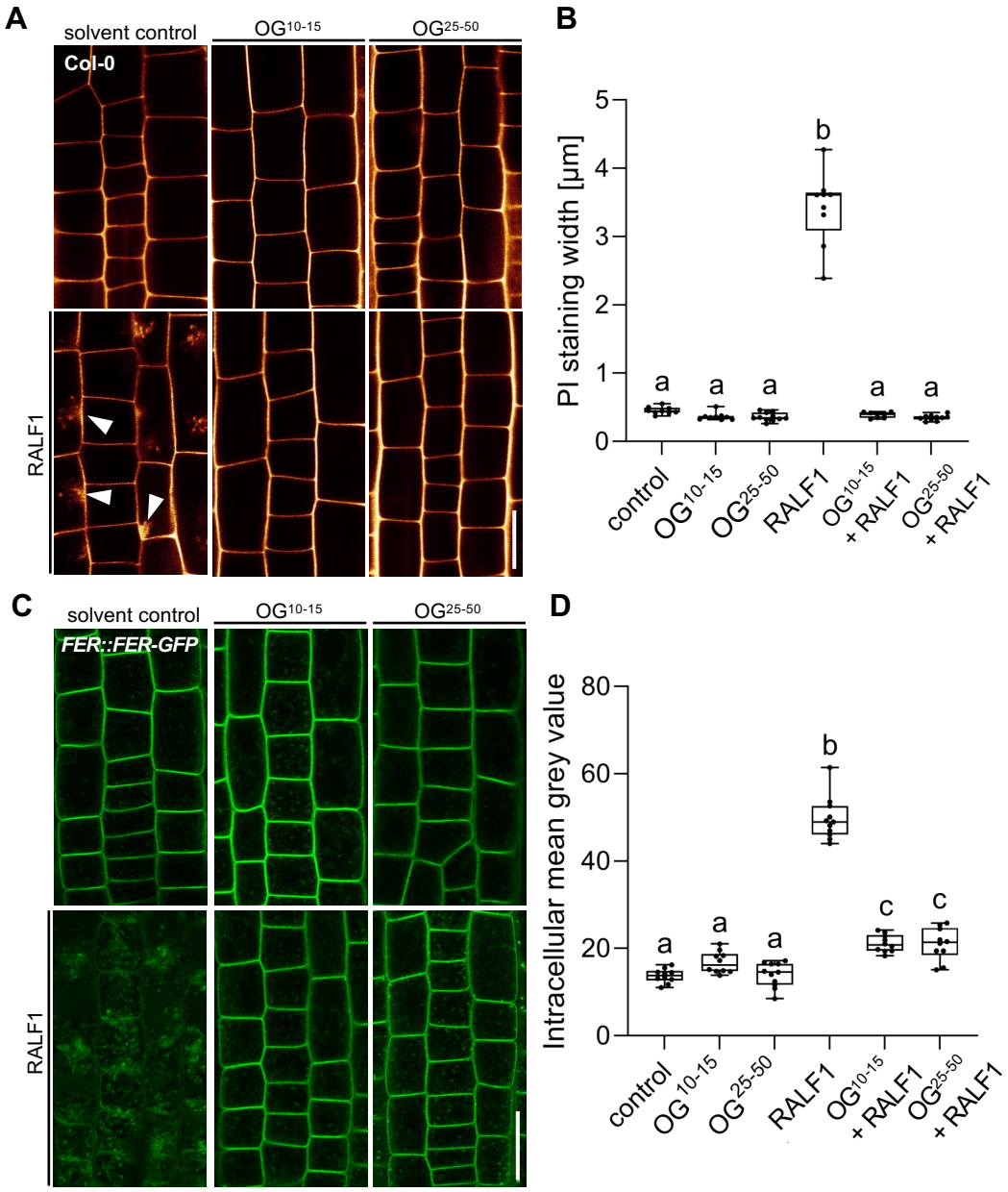
A
solvent control
OG10-15
OG25-50
Col-0
RALF1
B
PI staining width [µm]
5
4
3
2
1
0
b
a
a
a
a
a
control
OG10-15
OG25-50
RALF1
OG10-15 + RALF1
OG25-50 + RALF1
C
solvent control
OG10-15
OG25-50
FER::FER-GFP
RALF1
D
Intracellular mean grey value
80
60
40
20
0
b
a
a
a
c
c
control
OG10-15
OG25-50
RALF1
OG10-15 + RALF1
OG25-50 + RALF1

Figure S4.

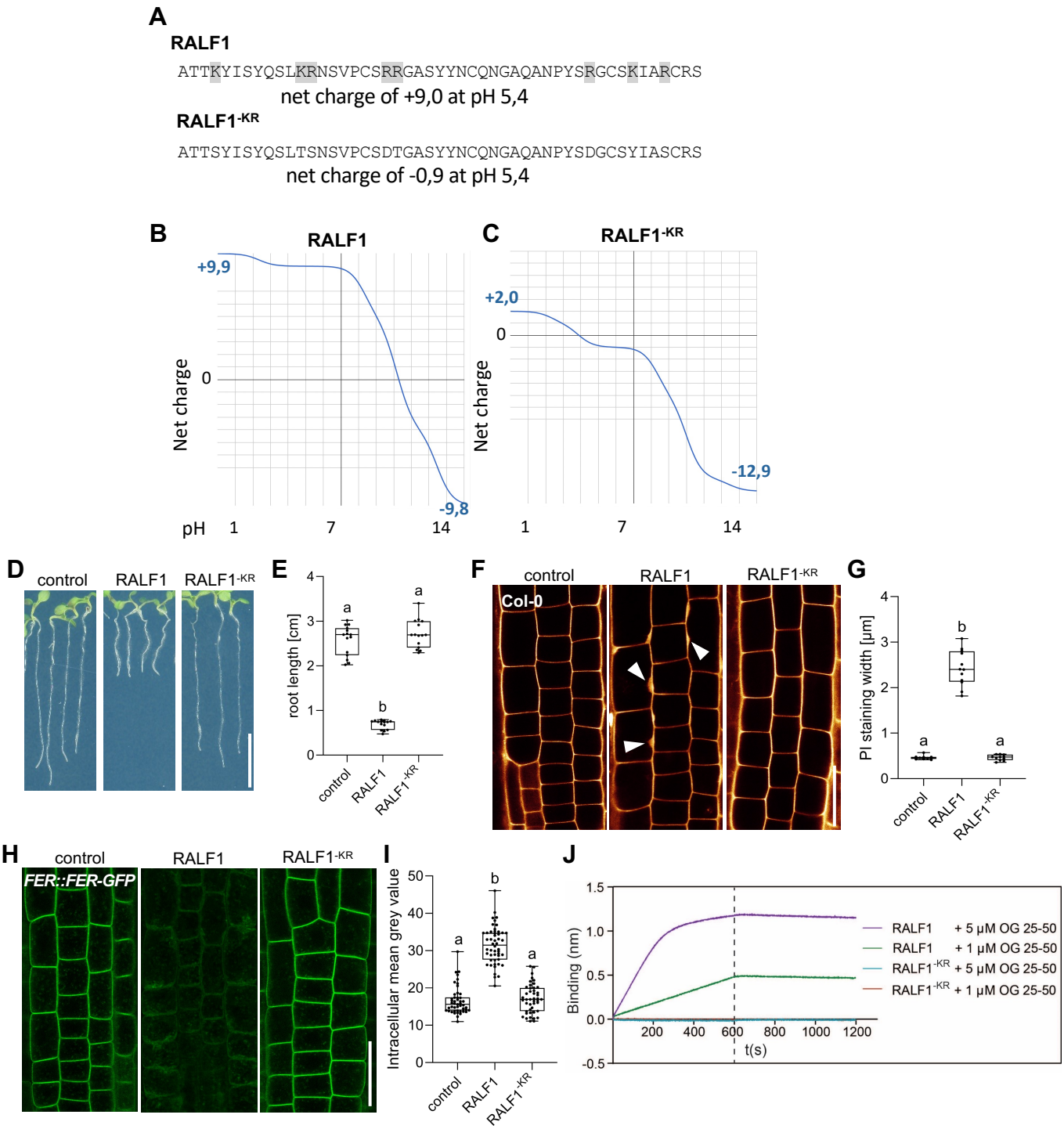
A
RALF1
ATTKYISYQSLKRNSVPCSRRGASYYNCQNGAQANPYSRGCSKIARCRS
net charge of +9,0 at pH 5,4
RALF1-KR
ATTSYISYQSLTSNSVPCSDTGASYYNCQNGAQANPYSDGCSYIASCRS
net charge of -0,9 at pH 5,4
B
RALF1
+9,9
0
-9,8
Net charge
pH 1 7 14
C
RALF1-KR
+2,0
0
-12,9
Net charge
1 7 14
D
control RALF1 RALF1-KR
E
root length [cm]
control RALF1 RALF1-KR
F
control RALF1 RALF1-KR
Col-0
G
PI staining width [µm]
control RALF1 RALF1-KR
H
control RALF1 RALF1-KR
FER::FER-GFP
I
Intracellular mean grey value
control RALF1 RALF1-KR
J
Binding (nm)
t(s)
RALF1 + 5 µM OG 25-50
RALF1 + 1 µM OG 25-50
RALF1-KR + 5 µM OG 25-50
RALF1-KR + 1 µM OG 25-50